Multi-Frequency Traction-to-Auxiliary Integrated EV Drivetrain: Eliminating the Need for an Auxiliary Power Module

1st Caniggia Viana
Department of Electrical Engineering
University of Toronto
Toronto, Canada
caniggiadiniz@gmail.com

2nd Mehanathan Pathmanathan
Department of Electrical Engineering
University of Toronto
Toronto, Canada
meha.pathmanathan@mail.utoronto.ca

3rd Peter W. Lehn
Department of Electrical Engineering
University of Toronto
Toronto, Canada
lehn@ecf.utoronto.ca

Abstract

Leveraging multi-frequency power transfer in the drivetrain, a solution is presented to eliminate the auxiliary power module in electric vehicles. The concept exploits energy harvesting from the drivetrain switching to achieve traction-to-auxiliary power transfer. Only a compensation capacitor, high-frequency transformer, diode rectifier, and a CL filter are added to the drivetrain. Simulations and experimental verification are conducted to validate the proposed system.

ACKNOWLEDGEMENT

This work was supported by the Natural Sciences and Engineering Research Council of Canada (NSERC) under Grant CRDPJ 513206-17.

Index Terms

Auxiliary power module, traction-to-auxiliary, electric vehicle, drivetrain, switching harmonic energy harvesting modeling.

I. Introduction

Electric vehicle (EV) adoption is significantly impacted by vehicle weight and production cost. While the former indirectly impacts range, a critical buyer concern, the latter directly affects the consumer choice [1]. The auxiliary power module (APM), included in EVs to supply auxiliary loads, contributes significantly with weight and cost, given its substantial and increasing power rating in modern EVs [2].

To mitigate these issues, two main strategies have previously been explored. Increasing the switching frequency of the APM allows for the use of smaller passive components, largely reducing the APM's total size [3], [4]. This approach has been proposed in the literature, although it may require special, and often expensive, wide-bandgap switches. Integration, wherein power electronic or passive components already present in the vehicle are leveraged to implement the APM, provides an alternative route to decrease the APM contribution to vehicle cost and weight [5]. In the literature, solutions have been investigated where a third winding and power electronic interface (PEI) are added to the OBC transformer [6], [7], [8]. Other solutions leverage the entire OBC as the primary side PEI of an isolated dc/dc converter, implementing the APM [9], [10]. A solution is proposed in [11], capable of implementing an APM without the need for a dedicated OBC. However, that solution is only suitable for dual inverter drivetrains, and cannot be utilized along with more conventional single inverter drives.

This work proposes a fully integrated traction-to-auxiliary (T2A) power supply, implemented by leveraging and controlling the zero-sequence component of the voltage applied to the machine, which eliminates the need for an APM. The proposed circuit possesses the following unique set of characteristics:

1) It can be implemented without the addition of any active switches, providing a cost-effective T2A solution. The additional circuitry is limited to a compensation capacitor, an isolation transformer, a diode rectifier, and a CL filter.
2) It does not require any specific OBC topology, making this a widely applicable solution.
3) When driving, no additional active switching action is required to operate the T2A system, resulting in no additional switching loss.
4) It harvests energy from the switching frequency component of the zero-sequence voltage and current in the drivetrain, a largely underutilized degree of freedom in the drivetrain. This increases the asset utilization ratio, allowing vehicle manufacturers to get more functionality out of the already deployed components.

II. Proposed Solution

The proposed solution consists of connecting the neutral point of the traction motor to the primary side of the T2A transformer, followed by the compensation capacitor, C_r. On the secondary side of the transformer, a center tapped diode rectifier is connected to a CL filter, followed by the low voltage (LV) battery.

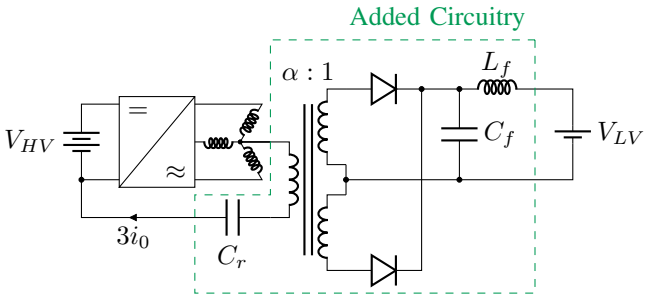

Fig. 1: Proposed T2A solution.

1) Operating Principle: The zero-sequence voltage, v_0, produced by the drivetrain, as described by the Clarke transformation. This voltage is defined as

$$v_0 = \frac{V_{HV}}{3} \sum_{i=a}^{c} g_i, \tag{1}$$

where g_i is the gating pulse associated with the top switch of leg "i" of the inverter, $i \in \{a, b, c\}$. The equivalent circuit representing the associated power transfer in Fig. 1 is shown in Fig. 2.

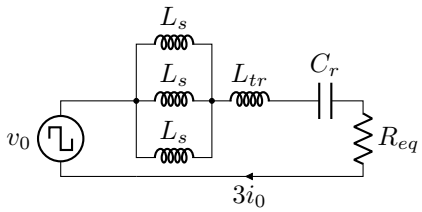

Fig. 2: Equivalent zero-sequence model of the proposed circuit.

In Fig. 2, L_s represents the zero-sequence (leakage) inductance of the machine, L_{tr} represents the leakage inductance of the transformer, referred to the primary side, and C_r is chosen to resonate, at the switching frequency, f_{sw}, with the loop inductance.

$$C_r = \left(\frac{1}{2\pi f_{sw}}\right)^2 \left(\frac{1}{L_{tr} + \frac{L_s}{3}}\right) \tag{2}$$

With placement of C_r defined by Fig. 2, the resonant nature of the circuit ensures the switching frequency component of the current dominates. Therefore, the power transfer in the circuit is related to the magnitude of the phasor describing the harmonic cluster around switching frequency of v_0, $\underline{V}^{(f_{sw})}$.

$$\underline{V}^{(f_{sw})} = \frac{2}{T_{sw}} \int_0^{T_{sw}} v_0\,(t)\, e^{-j2\pi f_{sw}} dt \tag{3}$$

In (3), T_{sw} is the switching period, $\frac{1}{f_{sw}}$. The objective of the control system is to control the magnitude of the voltage described in (3) without interfering with the driving operation.

A. Single Frequency Approximation

Note that (3) abstracts the effects of the cluster of frequency disturbances as a single-frequencies. While not exactly mathematically descriptive of the Fourier content of the zero-sequence voltage produced by this approach, this equation allows for power transfer control, provided that the impedance of the transformer is chosen such that

$$\frac{R_{eq}}{2\pi\left(L_{tr} + \frac{L_s}{3}\right)} < f_{sw} + 5f_r, \tag{4}$$

where f_r is the maximum electric frequency of the rotor. This design condition ensures that the LC filter hs wide enough bandwidth to allow the all frequency components in the cluster to produce significant currents.

III. Control System

In this paper, a SPWM modulator synthesizes the machine voltage requested by the drive control to track, for instance, a torque or speed reference. Sufficiently covered in the literature, the drive control is outside the scope of this work. Note, that the same approach applies even if injection of third harmonic is used to enable higher higher voltage synthesis.

As in regular drive systems, the space-vector representation of the voltage requested by the drive control is given, as a function of the modulation index, M, and modulation angle, θ, by

$$\vec{v^*} = \frac{V_{HV}}{2} M e^{j\theta}. \tag{5}$$

The modulator defines the gating pulses by comparing the modulating signals with an appropriate carrier. To implement the T2A controller, three carriers c_a, c_b, and c_c are defined, such that

$$\begin{bmatrix} g_a \\ g_b \\ g_c \end{bmatrix} = \begin{bmatrix} M\cos(\theta) > c_a \\ M\cos(\theta - 120°) > c_b \\ M\cos(\theta + 120°) > c_c \end{bmatrix}, \tag{6}$$

where a controllable phase-shift, $\delta \in [0°, 120°]$, is established between carriers, as shown in Fig. 3.

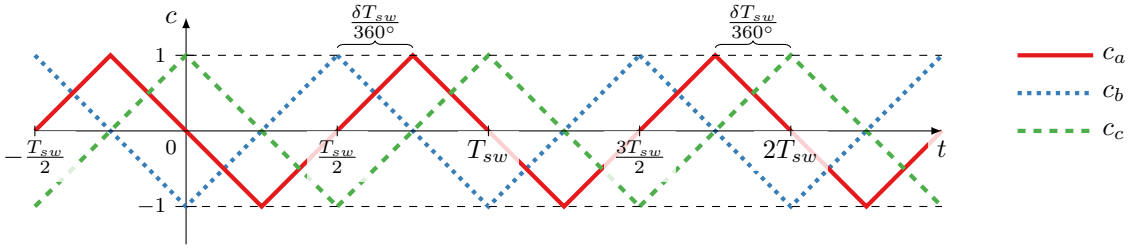

Fig. 3: Carrier definition and phase-to-phase carrier phase-shift representation.

The magnitude of the switching frequency component of the zero-sequence voltage is dependent on carrier phase-shift, δ, and can be shown to be approximately

$$\left|\underline{V}^{(f_{sw})}\right| \approx \left(\frac{2V_{HV}}{3\pi}\right) J_0\left(\frac{M\pi}{2}\right) \left|1 + 2\cos(\delta)\right|, \tag{7}$$

where J_0 is a Bessel function of the first kind. Equation (7) implies that the T2A power transfer can be controlled by varying δ. A value of $\delta = 0°$ leads to maximum voltage and consequent maximum power transfer, whereas $\delta = 120°$ brings T2A power output to 0. Fig. 4 shows how the magnitude of the combines frequencies clustered around the switching frequency vary as a function of the modulation index, M, and the carrier phase-shift, δ. Moreover, changing the carrier phase-shift does not affect the line-to-line voltages applied to the machine, hence, the system does not have any effect on the drive operation.

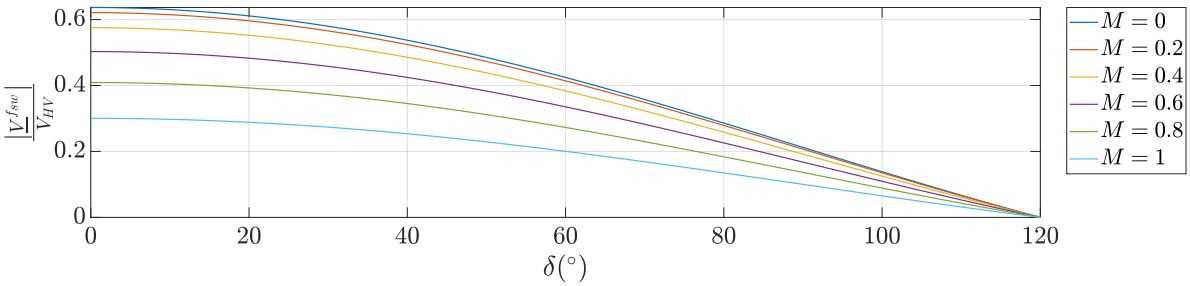

Fig. 4: Magnitude of the zero-sequence voltage produced around the switching frequency as a function of the modulation index and carrier phase-shift.

A control system is proposed using a simple PID controller to correct the value of delta to ensure i_{LV} tracks the associated reference, i^*_{LV}. This control loop runs in parallel with the traditional drive control. The T2A control diagram is shown in Fig. 5. The saturation block ensures $0° \leq \delta \leq 120°$.

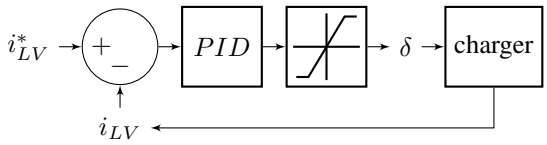

Fig. 5: Proposed T2A control loop, to be run in parallel with the drive control.

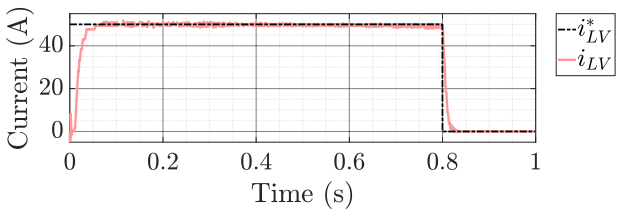

(a) T2A output current reference and T2A output current.

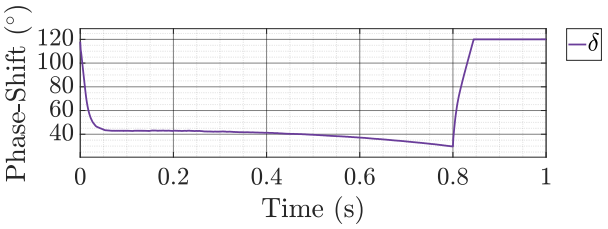

(b) Phase-to-Phase carrier phase-shift.

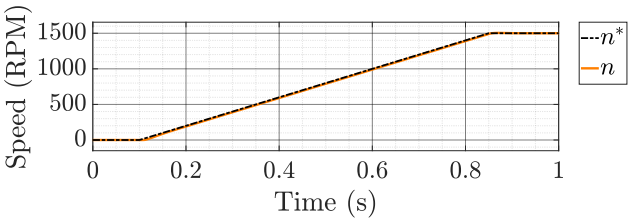

(c) Reference speed and speed.

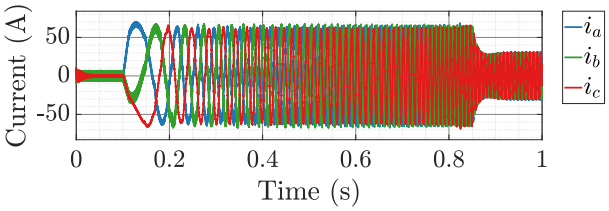

(d) Phase currents through the machine windings.

Fig. 6: Simulation results, showing simultaneous T2A and drive operation.

IV. Simulations

Using the control architecture described in Fig. 5, along with a traditional speed-tracking drive control, the system in Fig. 1 is simulated. The simulation results are shown in Fig. 6.

At time $t = 0$, the T2A output current reference is set to $i_{LV^*} = 50\ A$. The system satisfactorily tracks the reference, as shown in Fig. 6a. To achieve T2A power transfer, the T2A controller reduces δ, from 120°, which results in the lowest voltage $\left|\underline{V}^{(1)}\right|$, toward 0°, which results in the highest voltage, as shown in Fig. 6b.

At time $t = 0.1\ s$, the speed reference is ramped up to 1500 RPM. The traditional drive control increases the current reference and accelerates the system, tracking the speed reference, as shown in Fig. 6c. Importantly, the current output of the system, shown in Fig. 6d, is unremarkable and similar to what is expected in a regular drive system, demonstrating that the presence and operation of the T2A system do not affect the drive system in any significant way. As the speed increases, the modulation index, M, increases, leading to a requirement of a somewhat lower value of delta to maintain the same power level. This relationship is best seen in Fig. 6b, at $0.5\ s < t < 0.8\ s$.

At time time $t = 0.8\ s$ the T2A output current reference is stepped down to $0\ A$, which the T2A control tracks. Once again, both the T2A operation and transient are demonstrated to not impact the drive control.

V. Experimental Results

An experimental circuit is setup to verify the analytical claims. The experimental setup has three main parts:

1) The power electronics and controls.
2) The PMSM and dynamometer, enabling driving operation at a specifiable speed and torque.
3) The T2A added circuitry, including transformer, rectifier, and compensation capacitor.

Pictures of the experimental setup are shown in Fig. 7. The parameters used in this experiment are shown in Table I.

The auxiliary voltage used in this experiment is $V_{LV} = 6V$, enforced by an electronic load, emulating the auxiliary battery. Note that this is a scaled representation of the 12 V typically used in EVs. This voltage level was selected based on laboratory component availability.

Four experiments are conducted to demonstrate the operation of the circuit.

(a) Inverter and DSP.

(b) PMSM & dynamometer.

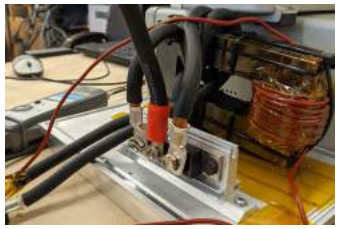

(c) Transformer & rectifier.

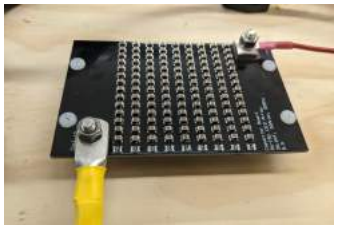

(d) Capacitor C_r.

Fig. 7: Experimental setup to be used for experimental verification.

TABLE I: Parameters used in experimental verification.

Description	Symbol	Value
System		
Battery Voltage	V_{HV}	400 V
Auxiliary Voltage	v_{LV}	60 V
Switching Frequency	f_{sw}	10 kHz
Machine		
0-Seq. Inductance	L_S	0.53 mH
q-axis Inductance	L_q	0.94 mH
d-axis Inductance	L_d	0.73 mH
Series Resistance	R_S	45 $m\Omega$
Pole Pairs	$p/2$	5
Flux Linkage	R_S	0.127 Wb
Rated Current (RMS)	I_{max}	200 A
T2A		
Transformer Inductance	L_{tr}	700 μH
Compensation Capacitor	C_r	280 nF
Turns Ratio	α	20 V/V
Filter Capacitance	C_f	4 mF
Filter Inductance	L_f	5.37 μH

1) T2A transient from 0 to 30 A output current reference at standstill.
2) T2A transient from 0 to 30 A output current reference while the drivetrain is operated at 500 RPM and 10 Nm output.
3) Steady-state T2A operation at 0 A output current at standstill.
4) Steady-state T2A operation at 30 A output current at standstill.

During the first experiment, the drivetrain is set to idle, i.e., to operate at 0 RPM and 0 Nm. With the T2A system initially outputting 0 current, a transient in reference output current, i^*_{LV}, is applied from 0 to 30 A. Auxiliary voltage and currents resulting from this experiment are shown in Fig. 8. The during the transient, the current rises to track the reference. The auxiliary voltage increases slightly, in the presence of current.

During the T2A transient, the current flowing through phase a of the machine is measured. The result is shown in Fig. 8. During the transient, the current remains approximately 0.

Using a torque transducer, the torque on the axle connecting the PMSM under test and the dynamometer is measured. The result is shown in Fig. 8. No significant transient can be observed in the torque during the T2A transient. This result suggests that the T2A system, despite leveraging the machine and drive inverter, has no significant impact on the mechanical behavior of the system.

The second experiment explored herein, similarly to the first one, applies a T2A transient in output current from 0 to 30 A. The difference between tests lies in the fact that the drive, here, is set to 500 RPM and 10 Nm. In this setup, the dynamometer is responsible for setting the system speed, while the drivetrain operates in torque control mode. The auxiliary current and voltage waveforms resulting from the aforementioned procedure are measured and shown in Fig. 9. As was observed in the test at standstill, the current rises to meet the reference, while the auxiliary voltage displays a slight increase.

The current flowing through phase a of the machine is measured during this operation. The result is shown in Fig. 9. It can be seen the the current is primarily sinusoidal, as a result of the drive operation. The ripple can be observed to be higher in the portion of the curve where the T2A system is processing zero power. This is the case because to produce $i_{LV} = 0$ the system applies approximately $\delta = 120°$ phase-shift, producing a significant line-to-line voltage component at $10kHz$. In contrast, to output $i_{LV} > 0$ the phase-shift is reduced, thereby reducing the line-to-line voltage component, but aligning the line-to-neutral

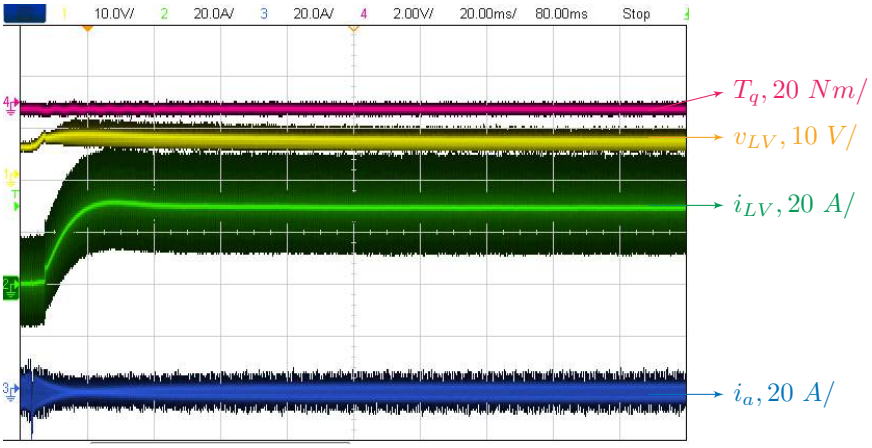

Fig. 8: Measured auxiliary voltage and currents, stator phase current, and drivetrain torque during T2A transient at standstill.

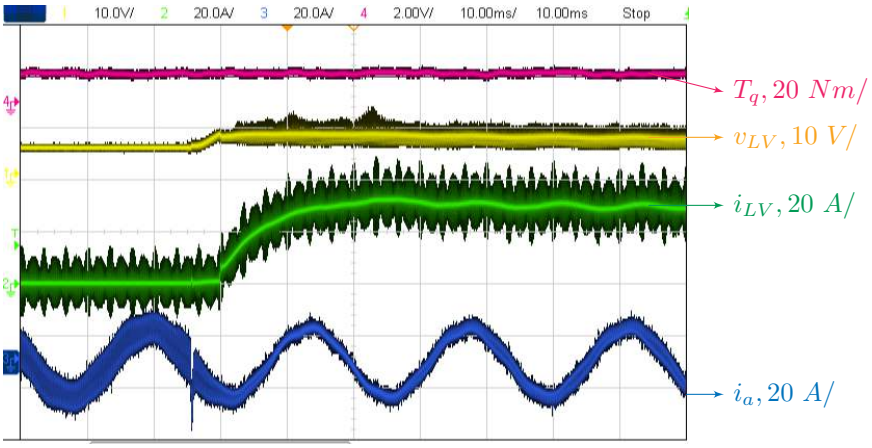

Fig. 9: Measured auxiliary voltage and currents, stator phase current, and drivetrain torque during T2A transient at 500 RPM and 10 Nm.

currents and voltages of all phases, thus increasing the current through neutral.

While the transient is applied, the measured torque remains at approximately 10 Nm. Once again, no appreciable transient is seen in the torque produced by the system. This result corroborates the analytical conclusion that the T2A system does not interfere with the drive mechanical behavior.

Two more experiments are conducted with the drive system at standstill. These tests aim to show that the system operates with less stator phase current ripple when outputting significant T2A power.

Firstly, the T2A system is set to operate at zero output current, $i^*_{LV} = 0$. The machine phase a stator current is measured. As shown in Fig. 10, the peak current value is around 7.5 A.

The previous experiment is repeated, but this time with the T2A system outputting $i_{LV} = 30\ A$. Fig. 11 shows the measured stator phase a current. In comparison with the no power case, this scenario produces less phase current ripple, with peak current below 5 A. This phenomenon is explained by the alignment of the phase-shift, decreasing the line-to-line voltage seen by the stator. In other words, to output power, the T2A system increases the 10 kHz component of the 0-axis current through the machine, but it reduces the 10 kHz component of $\alpha-$ and $\beta-$axis currents more than commensurately, thus reducing the phase current ripple in comparison to the zero output case.

VI. Conclusion

A traction-to-auxiliary power supply integrated to the drivetrain is proposed for electric vehicles. The solution leverages the switching frequency component of the zero-sequence current through the drive machine, a usually underutilized degree of freedom in the drive system, to facilitate power transfer. As a result, the electric vehicles requirement of an auxiliary power module, a significant component both in weight and in cost, is eliminated. In lieu of a standalone auxiliary power

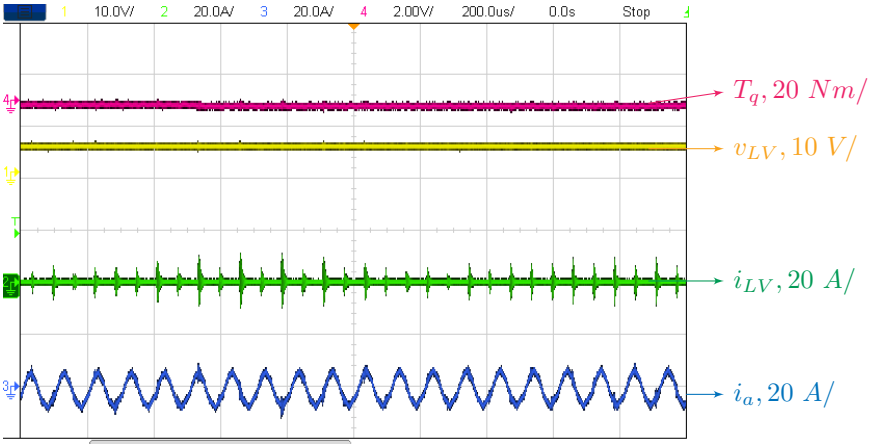

Fig. 10: Measured auxiliary voltage and currents, stator phase current, and drivetrain torque during steady-state operation at standstill, with zero T2A output power.

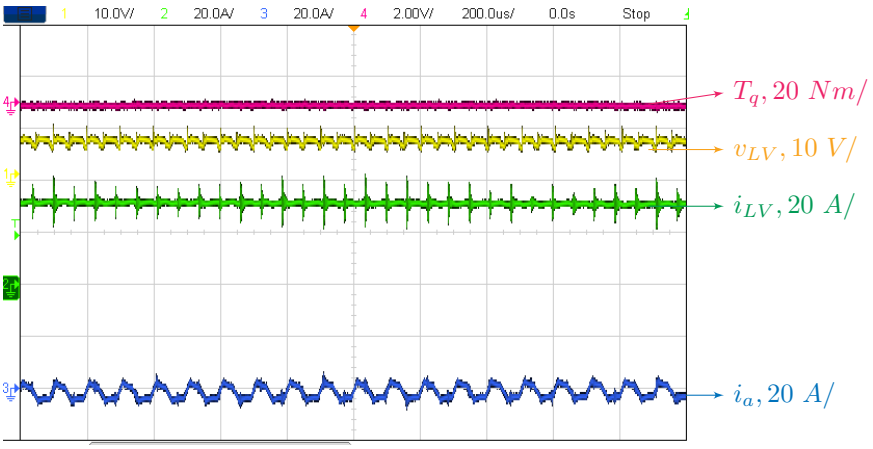

Fig. 11: Measured auxiliary voltage and currents, stator phase current, and drivetrain torque during steady-state operation at standstill, with zero T2A output power.

module, a small transformer and other small passive components are included. Despite using the zero-sequence component, this multi-frequency technique does not impede techniques that facilitate higher drive voltage synthesis, such as third harmonic injection.

Simulation results are presented to corroborate the analytical results, wherein the proposed auxiliary charger is demonstrated to operate simultaneously with the drive system. The operation is achieve by virtue of controlling the phase-shift between carriers in the drive system modulator, while not interfering with drive controls. An experimental setup is constructed and used to demonstrate not only satisfactory traction-to-auxiliary operation, but also that the additional system does not cause any noticeable interference with the mechanical behavior of the drivetrain, despite leveraging both the traction machine and the traction inverter during driving operation.

REFERENCES

[1] M. Coffman, P. Bernstein, and S. Wee, "Factors affecting EV adoption: A literature review and EV forecast for Hawaii," *Electric Vehicle Transportation Center*, no. April 2015, pp. 1–36, 2015.

[2] S. M. Hasan, M. N. Anwar, M. Teimorzadeh, and D. P. Tasky, "Features and challenges for Auxiliary Power Module (APM) design for hybrid/electric vehicle applications," *2011 IEEE Vehicle Power and Propulsion Conference, VPPC 2011*, 2011.

[3] A. M. Naradhipa, S. Kim, D. Yang, S. Choi, I. Yeo, and Y. Lee, "Power Density Optimization of 700 kHz GaN-Based Auxiliary Power Module for Electric Vehicles," *IEEE Transactions on Power Electronics*, vol. 36, no. 5, pp. 5610–5621, 2021.

[4] H. Moradisizkoohi, N. Elsayad, and O. A. Mohammed, "Experimental Demonstration of a Modular, Quasi-Resonant Bidirectional DC-DC Converter Using GaN Switches for Electric Vehicles," *IEEE Transactions on Industry Applications*, vol. 55, no. 6, pp. 7787–7803, 2019.

[5] A. Khaligh and M. Dantonio, "Global Trends in High-Power On-Board Chargers for Electric Vehicles," *IEEE Transactions on Vehicular Technology*, vol. 68, no. 4, pp. 3306–3324, 2019.

[6] L. Zhu, H. Bai, A. Brown, and L. Keuck, "A Current-fed Three-port DC/DC Converter for Integration of On-board Charger and Auxiliary Power Module in Electric Vehicles," *2021 IEEE Applied Power Electronics Conference and Exposition (APEC)*, pp. 577–582, 2021.
[7] Y. Tang, J. Lu, B. Wu, S. Zou, W. Ding, and A. Khaligh, "An Integrated Dual-Output Isolated Converter for Plug-in Electric Vehicles," *IEEE Transactions on Vehicular Technology*, vol. 67, no. 2, pp. 966–976, 2018.
[8] B. Farhangi and H. A. Toliyat, "Modeling and Analyzing Multiport Isolation Transformer Capacitive Components for Onboard Vehicular Power Conditioners," *IEEE Transactions on Industrial Electronics*, vol. 62, no. 5, pp. 3134–3142, 2015.
[9] J. G. Pinto, V. Monteiro, H. Gonçalves, and J. L. Afonso, "Onboard reconfigurable battery charger for electric vehicles with traction-to-auxiliary mode," *IEEE Transactions on Vehicular Technology*, vol. 63, no. 3, pp. 1104–1116, 2014.
[10] S. Kim and F. S. Kang, "Multifunctional onboard battery charger for plug-in electric vehicles," *IEEE Transactions on Industrial Electronics*, vol. 62, no. 6, pp. 3460–3472, 2015.
[11] C. Viana, M. Pathmanathan, and P. W. Lehn, "Auxiliary Power Module Elimination in EVs Using Dual Inverter Drivetrain," *IEEE Transactions on Power Electronics*, pp. 1-1, 2022.